Science Bulletin 70 (2025) 748–755

Contents lists available at ScienceDirect

Science Bulletin

journal homepage: www.elsevier.com/locate/scib

Article

Two types of heavy precipitation in the southeastern Tibetan Plateau

Dianbin Cao [a,b], Xuelong Chen [c,*], Deliang Chen [d], Yu Du [e], Yuhan Luo [e], Yang Hu [f], Qiang Zhang [c], Yaoming Ma [c], Fahu Chen [a]

[a] Alpine Paleoecology and Human Adaptation Group (ALPHA), State Key Laboratory of Tibetan Plateau Earth System, Environment and Resources (TPESER), Institute of Tibetan Plateau Research, Chinese Academy of Sciences, Beijing 100101, China
[b] Motuo Observation and Research Center for Earth Landscape and Earth System, Chinese Academy of Sciences, Linzhi 860712, China
[c] Land-Atmoshere Interaction and its Climatic Effects Group, State Key Laboratory of Tibetan Plateau Earth System, Environment and Resources (TPESER), Institute of Tibetan Plateau Research, Chinese Academy of Sciences, Beijing 100101, China
[d] Regional Climate Group, Department of Earth Sciences, University of Gothenburg, Gothenburg 40530, Sweden
[e] School of Atmospheric Sciences, Sun Yat-sen University, Southern Marine Science and Engineering Guangdong Laboratory (Zhuhai), Zhuhai 519082, China
[f] Ministry of Education Key Laboratory for Earth System Modeling, Department of Earth System Science, Tsinghua University, Beijing 100084, China

ARTICLE INFO

Article history:
Received 9 May 2024
Received in revised form 26 November 2024
Accepted 28 November 2024
Available online 25 December 2024

Keywords:
Southeastern Tibetan Plateau
Heavy precipitation
Atmospheric circulation patterns
Tibetan Plateau vortex type
Mid-latitude trough type

ABSTRACT

The southeastern Tibetan Plateau (SETP) is the preeminent summer heavy precipitation region within the Tibetan Plateau (TP). However, the large-scale circulation types and dynamics driving summer heavy precipitation in the SETP remain inadequately elucidated. Using the hierarchical clustering method, two distinctive atmospheric circulation patterns associated with heavy precipitation were identified: the Tibetan Plateau vortex type (TPVT, constituting 56.6% of the events) and the mid-latitude trough type (MLTT, 43.4%). A comprehensive examination of the two atmospheric circulation patterns reveals a clear nexus between the occurrences of summer heavy precipitation and positive vorticity anomalies, moisture convergence, as well as the southeastward displacement of the westerly jet core. Specifically, TPVT events are characterized by the eastward and dry-to-wet potential vorticity progression processes, while MLTT events are linked to the intrusion of a deep extratropical trough into the SETP. This study advances our understanding of the complex mechanisms governing the summer heavy precipitation in the SETP, shedding light on critical meteorological processes in the region.

1. Introduction

The Tibetan Plateau (TP), often referred to as the "Asian Water Tower" [1], is the source of Asia's major rivers, sustaining over a quarter of the global population [2,3]. Heavy precipitation plays a crucial role in replenishing water resources, local glacier mass balance and ecosystems on the TP [4–6]. Meanwhile, it can also often result in secondary disasters, such as mudslides and landslides, which are especially prevalent in the southeastern Tibetan Plateau (SETP) due to its geological vulnerability [7]. Heavy precipitation events in the SETP garner significant public attention due to their substantial impact on socio-economic aspects, and the safety of the local residents [8–10].

The spatial distribution of heavy precipitation across the TP displays a northwest-southeast gradient consistent with total precipitation, predominantly concentrating in the SETP during summer [7,11,12]. Heavy precipitation is determined by synoptic circulation regimes that regulate the dynamic and thermodynamic background fields [13–16], such as robust moisture transport [17–19], strong vertical ascent motion and instability conditions [20–22]. Previous studies have shown that regional heavy precipitation events on the TP can largely be caused by increased moisture originating from the Indian subcontinent, the Bay of Bengal, and the Arabian Sea during the summer monsoon season [11,23–25]. The meridional shift of the subtropical westerly jet stream can influence the location and intensity of precipitation [24,26]. Plateau shear lines are the dominant weather systems for the summer heavy precipitation over the SETP [9,27]. Furthermore, Rossby wave responses and tropical cyclone activity from the Bay of Bengal can also induce vorticity and water vapor transport anomalies, triggering heavy precipitation in the SETP [28–30].

The SETP occupies a unique geographical position at the convergence of various multiscale weather systems, including the Indian

* Corresponding author.
E-mail address: x.chen@itpcas.ac.cn (X. Chen).

https://doi.org/10.1016/j.scib.2024.12.031

monsoon, subtropical westerly jet stream, plateau shear line, plateau vortex, subtropical high pressure, and Rossby wave trains [16,24,25,31]. These intricate weather systems collectively foster robust updrafts and extensive regional moisture convergence. However, prior research has primarily concentrated on elucidating precipitation trends [32,33], precipitation intensity [10,34], orographic impacts on the precipitation [13,35], water vapor transport and vortex systems related to heavy precipitation in the SETP [31,36–39]. Up to now, few studies have discussed the relationship between circulation configuration and regional heavy precipitation in the SETP [16,24]. There remains a notable gap in our understanding of the dominant circulation configurations and evolutionary processes governing the summer heavy precipitation events in the SETP [24,25,40]. Accurately forecasting the heavy precipitation events in the SETP continues to pose a significant challenge [41,42].

The objectives of this study are twofold: firstly, to categorize the weather circulation systems responsible for heavy precipitation events in the SETP, and secondly, to explore the underlying mechanisms giving rise to the heavy precipitation events.

2. Datasets and methodology

2.1. Datasets

Quality-controlled daily rain-gauge records at 120 meteorological stations on the TP in the summer (June-July-August, JJA) of 1980–2014 were collected by this study from the China Meteorological Administration. Valid precipitation events were identified as those with daily precipitation rates exceeding 0.1 mm d^{-1} [43]. Fig. 1a provides an overview of the spatial distribution of the summer mean precipitation recorded at observation sites across the TP. Notably, regions with precipitation exceeding 300 mm were primarily situated within the SETP. Precipitation gradually decreases when moving towards the northwestern TP.

To perform synoptic classifications and diagnostics, daily atmospheric parameter datasets including geopotential height, horizontal winds, vertical velocity, air temperature, surface pressure, and specific humidity for the years of 1980–2014 were employed. They were acquired from the National Aeronautics and Space Administration Modern-Era Retrospective Analysis for Research and Applications dataset, Version 2 (MERRA-2), with a horizontal resolution of 0.5° × 0.625°. MERRA-2 has undergone extensive validation and been widely verified to be reliable in delineating atmospheric circulation over the TP [44–46]. These datasets are accessible at https://disc.gsfc.nasa.gov/datasets/.

2.2. Methodology

2.2.1. Study region and definition of summer heavy precipitation

The SETP was defined as the geographical area encompassing coordinates within 27°–32°N latitude and 90°–102°E longitude, a delineation referenced in previous studies [47,48]. A heavy precipitation event in the SETP was defined as the day when the regional mean daily precipitation equaled or exceeded the 90th percentile (a threshold value of 9.1 mm d^{-1}) of the regional mean daily precipitation series during 1980–2014. More details regarding this method have been described in previous studies [9,49,50]. Using this criterion, a total of 316 summer heavy precipitation samples were obtained, which contributed 23.78% of the summer mean precipitation in the region, as illustrated in Fig. 1b. The contributions of the two moderate-intensity precipitation events (falling within the 50th to 75th and 75th to 90th percentile ranges) to summer mean precipitation were 28.55% and 25.19%, respectively (Fig. 1b). That of light precipitation was 22.48%.

2.2.2. Calculations of moisture flux convergence, stream function, and velocity potential

The moisture flux convergence (MFC) is calculated as follows:

$$\mathrm{MFC} = -\int_{p_s}^{p_t} \nabla_p \cdot \left(\vec{v}q\right)\frac{dp}{g}, \tag{1}$$

where MFC is the horizontal moisture flux convergence integrated from the surface to the top of the atmosphere. p is pressure. p_s and p_t are the surface pressure and top level (300 hPa) pressure, respectively. $\vec{v}(u,v)$ is the horizontal wind vector, q is the specific humidity, and g is the gravitational acceleration.

In addition, the stream function and velocity potential were used in the analysis to better identify and understand the motion characteristics of atmospheric fluids. A 2-D flow can be decomposed into two scalar functions: stream function $\psi(x,y)$ associated with its rotational property and velocity potential $\varnothing(x,y)$ associated with its divergent property. The mathematical relationship with the velocity field:

$$\vec{v} = \vec{\nabla}\varnothing + \vec{\nabla} \times \psi, \tag{2}$$

2.2.3. Hierarchical clustering

To objectively classify the large-scale circulation patterns of the summer heavy precipitation samples in the SETP from 1980 to 2014, a hierarchical clustering algorithm was employed. This

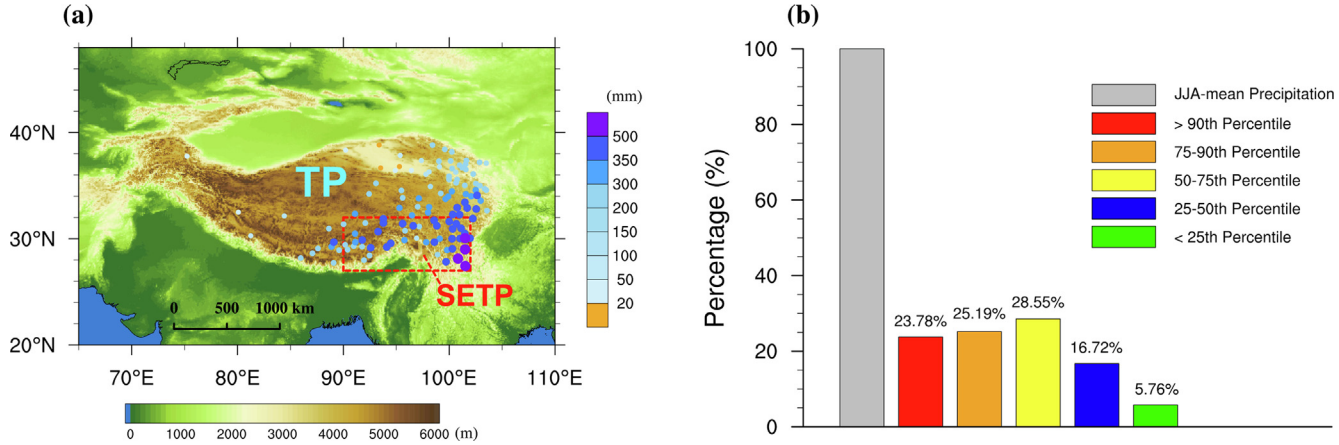

Fig. 1. (a) Topography (colored) in the Tibetan Plateau and adjacent areas. Solid colored dots indicate the locations of observation stations and JJA-mean precipitation (unit: mm) during 1980–2014. The red rectangle is the SETP analysis region in this study. (b) Contribution (unit: %) from the five classifications of daily precipitation intensity (<25th, 25–50th, 50–75th, 75–90th, and >90th percentile) to the JJA-mean precipitation in the SETP. The percentage values are marked on the five bars.

method has been widely utilized in atmospheric circulation classification studies [50–53]. The classification was based on the daily geopotential height at 500 hPa over a defined region, spanning 5°–50°N latitude and 60°–130°E longitude. The 500 hPa pressure level is near to the TP's surface height, which is susceptible to various atmospheric circulation systems (e.g., plateau vortex, Rossby wave, Indian monsoon and North Pacific subtropical high) [31]. We also tested the sensitivity of clustering results to the size of the defined region. It demonstrated that the atmospheric circulation classification was insensitive to the variation of defined region size in this study (Fig. S1 online).

The clustering process began by treating each daily geopotential height field on heavy precipitation days as an individual cluster. Subsequent clusters were formed by randomly selecting two original clusters and calculating Ward's distance (WD), following Ward's method [54]. WD is defined as the increment in the error sum of squares (ESS) after the formation of a new cluster by combining two randomly selected original clusters (i.e., $WD = ESS_{new} - ESS_{ori1} - ESS_{ori2}$), which represents the dissimilarity between the two clusters. Here, ESS is calculated as follows:

$$ESS = \sum_{i=1}^{n} |P_i - P_a|^2, \quad (3)$$

where P_i is the daily geopotential height within the cluster, P_a is the average of the cluster, and n is the number of samples. When the WD value experiences a radical jump (WD increment >5 times the standard deviation), the circulation features of the two clusters are disparate, and the merger should be terminated (Fig. S1c1 online); and vice versa. Finally, all the main circulation clusters were identified for the heavy precipitation in the SETP. Additional details about the methodology have been described in previous studies [50,52].

3. Results

3.1. Circulation types associated with the summer heavy precipitation

The application of the hierarchical clustering method has yielded two distinct types of circulation patterns associated with the heavy precipitation in the SETP. The two types of heavy precipitation have mean intensities of 9.3 mm d^{-1} and 9.2 mm d^{-1}, respectively. Type 1 comprises 56.6% of all heavy precipitation samples, and Type 2 is 43.4%. They constitute 13.4% and 10.4% of the summer mean precipitation for the SETP. There are notable heavy precipitation values concentrate within the SETP and lower values spread in the rest of the TP, when we demonstrated averaged precipitation intensity for the two types in Fig. S2 (online). These results indicate that the two circulation types classified by the method are able to represent the characteristics of regional heavy precipitation in the SETP well.

Fig. 2a, b show composites of the geopotential height at 500 hPa (represented by solid blue and pink contours) for each type. Type 1 is characterized by a cyclonic vortex system (indicated by the pink line in Fig. 2a) positioned over the SETP. The vortex system is accompanied by pronounced horizontal wind shears and elevated specific humidity levels in the SETP (the regional mean specific humidity for the SETP is 6.4 g kg^{-1}). In the central region of the Indian Peninsula, a cyclonic circulation is evident. The cyclone causes a warm and humid southerly flow on its right side. This southerly flow splits into two branches when it moves northward. One branch turns into an easterly airflow at the foot of Himalaya mountains and the other branch transits into a southwesterly airflow directed towards the SETP (as indicated by the black dashed lines in Fig. 2a).

Type 2 exhibits some similarities to Type 1 in that the SETP is also influenced by a vortex system, a conspicuous wind shear band, and a high regional mean specific humidity of 6.1 g kg^{-1}. However, notable differences arise in the cyclonic circulation over the Indian Peninsula between the two types. The cyclonic circulation over the SETP for Type 2 is relatively weaker compared to Type 1, and the center of the Indian low-pressure system is located further to the north. Within the northeastern quadrant of the Indian low-pressure, a robust southerly flow transports moisture from the Bay of Bengal to the SETP, without the easterly airflow branch seen in Type 1 (as denoted by the black dashed line in Fig. 2b). The southerly moisture transport is also reported in the formation of spring precipitation on the Hengduan mountain [55]. Furthermore, significant disparities between the two types also emerge in the mid-latitude region. Type 2 features a strong mid-latitude cyclone located in northeastern China, accompanied by a flat westerly airflow on its western side (Fig. 2b). The mid-latitude of Type 1 has a circulation pattern of two troughs and one ridge. One shallow trough is situated on the northwestern side of the TP, while the other trough is located over the northeastern part of China (highlighted by brown dashed lines in Fig. 2a). The ridge is positioned in the longitude zone near Lake Baikal.

In order to show the unique relationship between the two circulation types and the heavy precipitation in the SETP, we also did the analysis of the weather circulation types for the four daily precipitation intensities (<10th, 45–55th, and 80–90th, and >90th percentile) in the SETP (Fig. S3 online). The circulation for the type 1 (Fig. S3a1 online) of the weak precipitation events (daily precipitation <10th percentile) exhibits an anticyclone over the SETP, which prevents moisture convergence to the SETP. Type 2 of the weak precipitation (Fig. S3a2 online) has a southerly flow with low water vapor content to the SETP. The averaged humidity in the SETP for the weak precipitation is around 4.3 g kg^{-1}. There were no cyclonic eddy activities on the TP when the two types of weak precipitation happened. The regional mean water vapor conditions for the moderate precipitation events, in the 45–50th and 80–90th percentiles, are 5.7 and 6.1 g kg^{-1}, respectively. Eddy activities occurred over the northwestern TP for the moderate precipitation (Fig. S3b1–b3, c1–c2 online). A distinct eddy activity occurred in the SETP during the heavy precipitation events (>90th percentile). The averaged humidity in the SETP for heavy precipitation is about 6.25 g kg^{-1} (6.4 g kg^{-1} for Type 1 and 6.1 g kg^{-1} for Type 2 in Fig. 2a, b, respectively), which is not significantly higher than those of the moderate precipitation. The comparison of water vapor and cyclonic eddy activity among the four precipitation intensities indicates that dynamic condition may play a more important role than water vapor in the formation of summer heavy precipitation in the SETP.

3.2. Circulation anomalies associated with the summer heavy precipitation

Fig. 2c, d show the composite anomalies of geopotential height, wind, and specific humidity at 500 hPa for Type 1 and Type 2 heavy precipitation. Type 1 has a notable feature of a closed cyclone with a horizontal spatial scale of 400–1000 km, commonly known as the Tibetan Plateau Vortex (TPV). This cyclonic TPV controls the weather over the SETP during heavy precipitation. Surrounding the TPV, an extensive anticyclonic circulation anomaly was observed over the west side of Lake Baikal, along with a relatively weaker anticyclonic anomaly situated over the northern Bay of Bengal. The maximum specific humidity anomaly is located over the SETP and its immediate surroundings, while negative specific humidity anomalies are evident on both sides (Fig. 2c).

Type 2 demonstrated a strong mid-latitude cyclone anomaly positioned over northeastern China. A cold trough at 500 hPa, extending from the cyclone (as indicated by the brown dashed line in Fig. 2b), stretches into the SETP, forming a weak trough anomaly

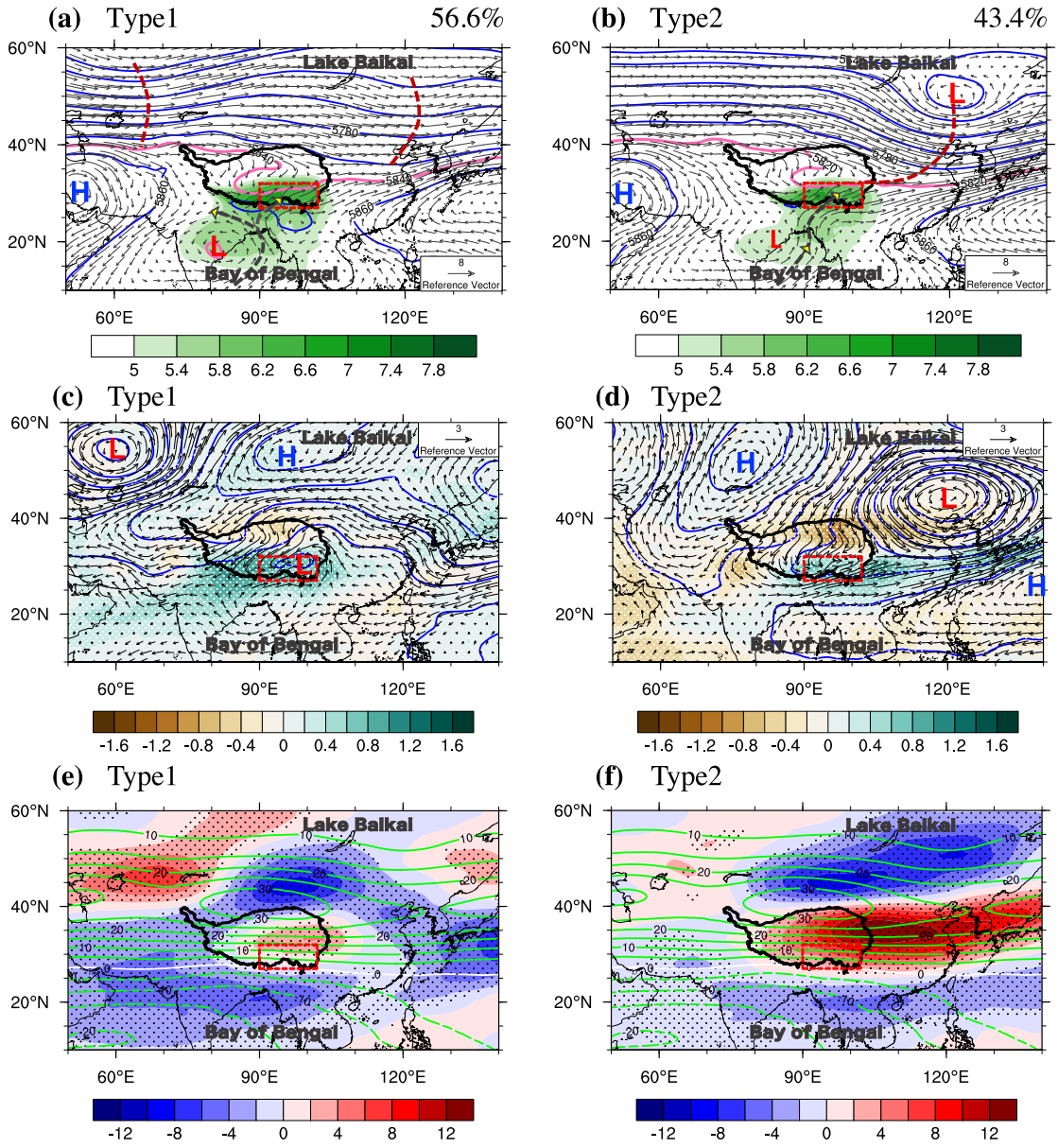

Fig. 2. Atmospheric circulation configurations related to the summer heavy precipitation in the SETP during 1980–2014. Composites of geopotential height (blue and pink solid contours, units: gpm), wind (vectors, units: m s^{-1}), and specific humidity (shading, units: g kg^{-1}) at 500 hPa for Type 1 (a) and Type 2 (b). The brown (black) dashed lines indicate trough (airflow) lines. (c) and (d) are the same as (a, b) except for the composite anomalies. (e) and (f) show the climatology (green contours) and anomalous (shading, units: m s^{-1}) of U-wind at 200 hPa. The black line (red rectangle) shows the elevation of 2500 m (the SETP). Areas significant at the 0.05 level are denoted by dots.

that resembles a tail shape. A corresponding anticyclonic anomaly is apparent on the western side of the mid-latitude cyclone. The northerly wind between these geopotential height anomalies facilitates the transport of cold polar air from high latitude regions to the SETP. Additionally, the anomaly associated with the western North Pacific subtropical high pressure, located near 20°N, extends towards the Bay of Bengal. Southwesterly winds on the western flank of this high-pressure system bring warm and moist air to the SETP. The south warm and moist air converges with the north cold air in the SETP, leading to the heavy precipitation in the SETP (Fig. 2d). It is worth noting that the cyclonic circulation over northeastern China and the western North Pacific subtropical high anomaly also create strong water vapor convergence over the Yangtze River Basin in China, forming a distinctive belt-like high specific humidity zone, which is notably different from Type 1.

The composite anomalies of U-wind fields at 200 hPa (Fig. 2e, f) reveal varying upper-level jet patterns in Type 1 and Type 2. The climatological jet core is situated on the northern side of the TP, near 40°N. For Type 1, the U-wind anomaly exhibits a tri-polar structure in East Asia. The jet core shifts southeastward, reaching around 35°N, and the SETP is positioned at the right entrance of the upper-level jet. The positioning of the jet core anomaly over the TP for Type 2 is similar to that for Type 1, but the westerly anomaly is more pronounced and extends further eastward towards Japan. According to the theory of geostrophic deviation [56], this upper-level configuration enhances high-level mass

divergence over the SETP, which, when combined with low-level convergence (Fig. 3a3, d3), contributes to intensified upward vertical motion and the transport of water vapor in the lower troposphere (Fig. 3b3, e3). These factors collectively result in heavy precipitation in the SETP region.

Although Type 1 and Type 2 have similar vortex systems on the TP (Fig. 2a, b), their composite anomalies have big differences (Fig. 2c–f). This means that heavy precipitation for the two types may derive from different evolution pathways. We will give a detailed analysis of the circulation development in the next section.

3.3. Occurrence and development of circulation types causing the heavy precipitation

To delve deeper into the evolution of heavy precipitation circulations in both Type 1 and Type 2, we examine the lead-day fields of various atmospheric variables, including velocity potential (Fig. S4 online), stream function (Fig. S5 online), geopotential height, temperature, water vapor flux, UV-wind, and specific humidity (Fig. 3 and Fig. S6 online).

For Type 1, the composite analysis of velocity potential and stream function at 500 hPa reveals the following evolution. A weak convergence initiates over the northwestern TP and subsequently strengthens while moving towards the SETP (Fig. S4a1–f1 online). A TPV is generated over the western TP, and reaches its maximum intensity at the onset of heavy precipitation (Fig. S5a1–f1 online). Prior to the formation of the TPV, a positive temperature anomaly at 500 hPa is consistently observed over the western TP. Two cyclonic circulation anomalies develop over the northern continent of the Arabian Sea and central India (Fig. 3a1). One specific humidity center forms over northern India due to the easterly moisture transport of the central India cyclonic circulation (Fig. S6a–c online).

A near-surface warm center on the western TP is important to the formation and development of a cyclonic vorticity [45,57]. Since the isentropic surfaces surrounding the near-surface warm center tilt downward to the center, when the air parcel adiabatically converges toward the center, it slides downward along the isentropic surfaces, and its potential vorticity experiences restructuring. Its static stability decreases and the baroclinity increases, leading to the development of the vertical vorticity [58]. In addition, the cyclonic disturbance over the northern continent of the Arabian Sea moves eastward over the western TP (Fig. S6a–c online). This leads to a southwesterly anomaly (Fig. S6 online), and increases the vertical movement and vertical water vapor transport along the southwest margin of the TP (Fig. 3c1, c2). Subsequently, the water vapor advection via the southwesterly flow penetrates the southwestern TP and converges there (Fig. 3a2, b2, c2) through the up-and-over moisture transport mechanism [59]. The dry dynamic (adiabatic slantwise vorticity development) and wet thermodynamic processes (moisture convergence and latent heat release) jointly lead to the generation and development of the TPV, which has been described by Wu et al. [45]. The TPV further develops and moves eastward to the SETP (Fig. S5d1–f1 online) under the background of the westerly winds. In addition, it can be clearly seen that the moisture is continuously transported northward to SETP from northern India and the Bay of Bengal due to the suction effect of the developed TPV (Fig. 3b2, b3). The latent heat release due to the updraft of wet air caused by the TPV further enhances the vertical motion and the suction effect. The latent heat release and supply of moisture form a positive feedback for the TPV growth. Hereby, the initial dry dynamic and subsequent wet thermodynamic processes are both responsible for the development and enhancement of the TPV, which leads to the occurrence of heavy precipitation in the SETP.

The origin and development of circulation patterns for Type 2 heavy precipitation events are notably distinct from those of Type 1, which testify that the classification based on the hierarchical clustering method is reasonable. The key differences between these two types are concluded as the following three aspects:

(1) Velocity potential and convergence: in Type 2, a weak convergence initially forms over the northern-central TP (Fig. S4a2 online). This convergence gradually intensifies and propagates from north to south across the TP in the velocity potential field (Fig. S4b2–f2 online).
(2) Mid-latitude circulation: in the mid-latitude region, both anticyclonic and cyclonic circulations emerge in the west and east, respectively (Fig. 3d1). This mid-latitude circulation pattern evolves along with the westward expansion of the western North Pacific subtropical high system in the stream function field (Fig. S5a2–f2 online).
(3) Temperature and moisture anomalies: distinct temperature and moisture anomalies are observed over the TP. There is a cold anomaly over the western TP and a warm anomaly over the eastern-central TP (Fig. 3d1). This temperature distribution differs significantly from that observed in Type 1 events (Fig. 3a1).

The circulation associated with Type 2 heavy precipitation originates from the development of a mid-latitude trough-ridge distribution. This atmospheric configuration leads to three critical meteorological processes:

(1) Southward transport of cold polar air: the mid-latitude trough-ridge pattern drives the southward transport of cold polar air from high-latitude regions toward the SETP. This results in a gradual decrease in temperature from north to south (Fig. 3d1–d3) over the TP.
(2) Interaction with Indian monsoon: as the cold air encounters the warm and humid southwesterly airflow associated with the Indian summer monsoon, it leads to the convergence of cold and warm air masses. This convergence results in the moisture compensation (Fig. 3e1–e3), formation of cyclonic shear lines (Fig. 3d2, d3) and enhancement of vertical motion (Fig. 3f1–f3).
(3) Westward extension of the western North Pacific subtropical high: the westward extension of the western North Pacific subtropical high system (Fig. S5a2–f2 online) further strengthens the southwesterly winds on its west side. This enhanced moisture transport contributes to vorticity development, primarily through the wet process, including the positive feedback process of latent heat release.

Collectively, these meteorological processes associated with the mid-latitude trough-ridge pattern, Indian monsoon, and the western North Pacific subtropical high system jointly led to the formation of Type 2 heavy precipitation in the SETP.

4. Conclusions and discussion

This study investigates the classifications and dynamical evolution of dominant circulation types related to summer heavy precipitation in the SETP. Two pathways connecting summer heavy precipitation events to synoptic circulation regimes in the SETP were firstly proposed in this study. Fig. 4 describes the distinct meteorological processes for the two types.

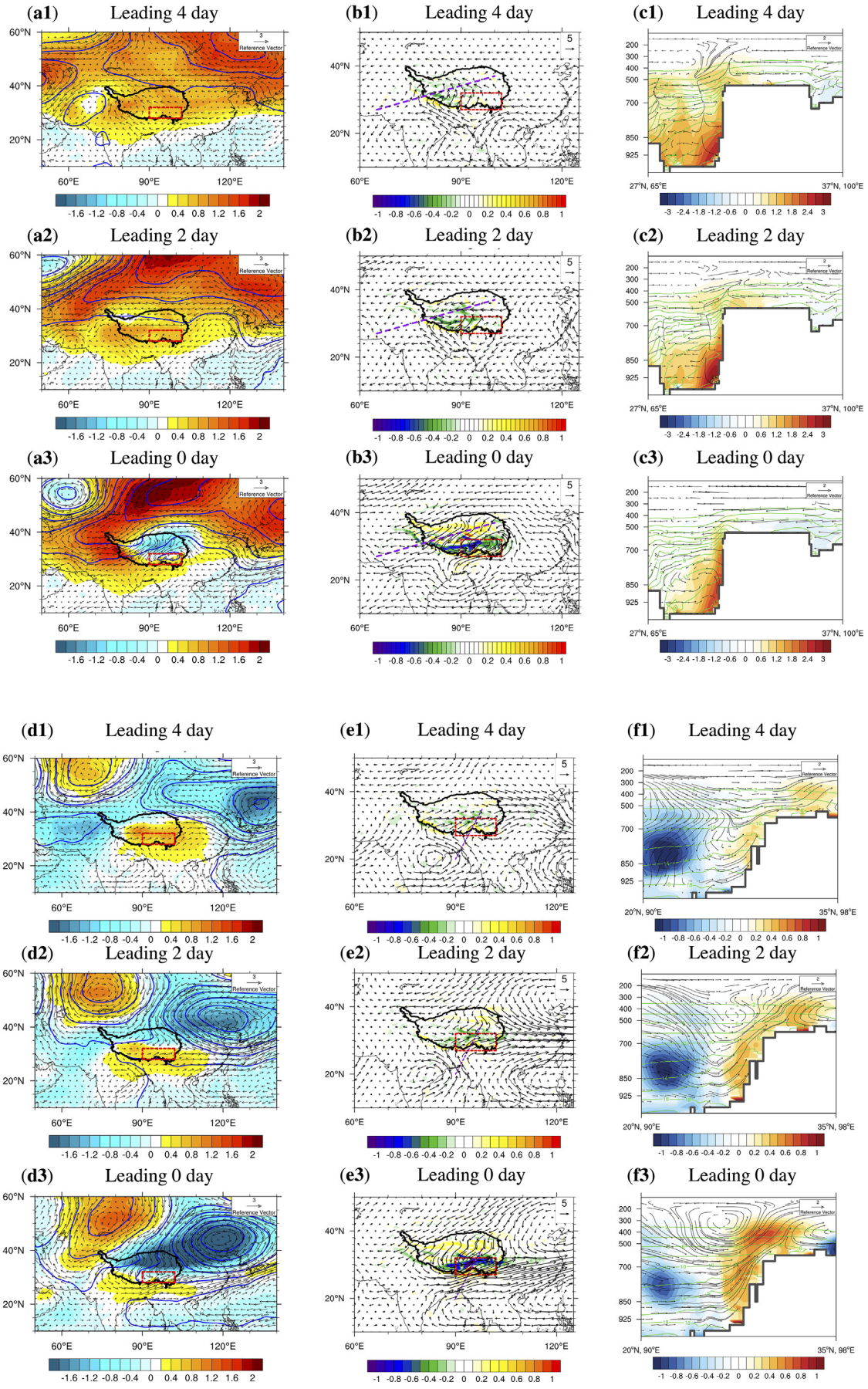
(a1) Leading 4 day
(b1) Leading 4 day
(c1) Leading 4 day
(a2) Leading 2 day
(b2) Leading 2 day
(c2) Leading 2 day
(a3) Leading 0 day
(b3) Leading 0 day
(c3) Leading 0 day
(d1) Leading 4 day
(e1) Leading 4 day
(f1) Leading 4 day
(d2) Leading 2 day
(e2) Leading 2 day
(f2) Leading 2 day
(d3) Leading 0 day
(e3) Leading 0 day
(f3) Leading 0 day
Reference Vector
60°E 90°E 120°E
60°N 40°N 20°N
27°N, 65°E 37°N, 100°E
20°N, 90°E 35°N, 98°E

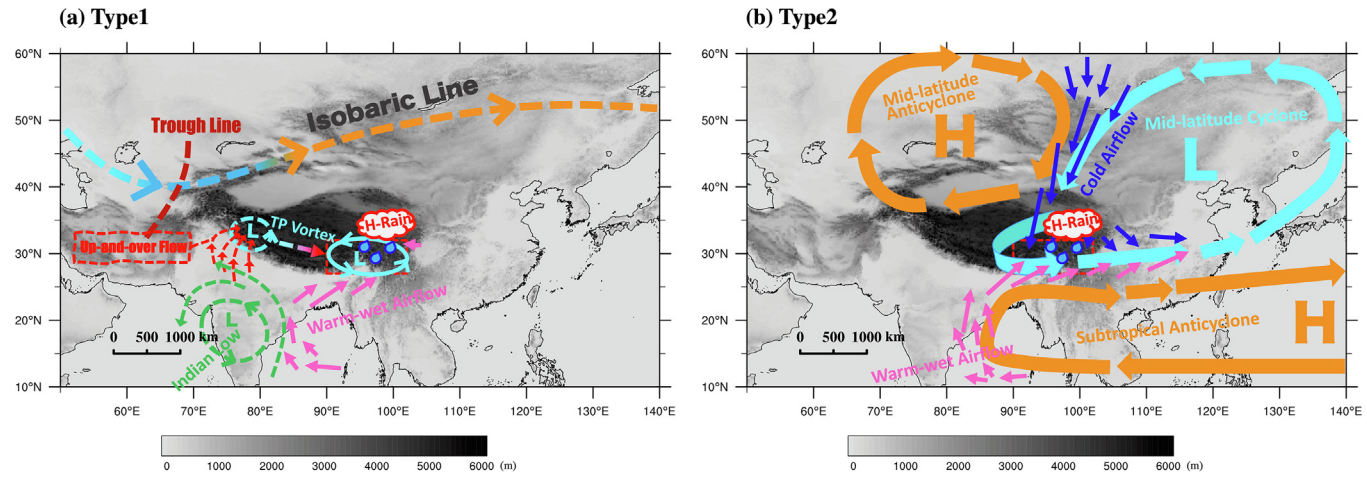

Fig. 4. Formation diagrams of summer heavy precipitation in the SETP. (a) Type 1. (b) Type 2. "H" and "L" denote high- and low-pressure systems, respectively, while arrow curves represent the atmospheric circulation.

Tibetan Plateau vortex type (TPVT): This type is linked to the generation of the TPV, which is triggered by the TP sensible heat. The formation of TPVT heavy precipitation is characterized by processes such as potential vorticity development and up-and-over moisture transport across the western TP. These processes drive the development of the TPV and its southeastward movement towards the SETP, which finally result in TPVT heavy precipitation.

Mid-latitude trough type (MLTT): This type is directly influenced by the mid-latitude circulation systems. A strong mid-latitude trough and ridge pattern drives the southward flow of cold air from middle and high latitudes toward the SETP, converging with warm and humid air transported through the Indian summer monsoon and the westward-extended Western Pacific subtropical high. The interaction between mid-high latitude and subtropical air masses, along with their circulation patterns, led to the MLTT heavy precipitation.

Previous studies have highlighted the association of SETP heavy precipitation with plateau wind shear in the lower troposphere [9], water vapor transport anomalies in the Bay of Bengal, and the westward extension of the Western Pacific subtropical high [16,25,60]. Our circulation analysis also reaffirms the importance of water vapor transport anomalies in the Bay of Bengal, and the westward extension of Western Pacific subtropical high. However, the causes of the wind shear line and the underlying mechanisms driving weather circulation anomalies are not clear in previous studies. Here we have clarified that the wind shear line was caused by the development and eastward movement of the plateau vortex generated in the western TP, and the invasion of the mid-latitude trough into the SETP. The mid-latitude wave activity and the abnormal extension of Western Pacific subtropical high collectively lead to the heavy rainfall belt spread from the SETP to the Yangtze River basin in China. In addition, it would also be interesting to look at the frequency changes of these two heavy precipitation types. There are no significant trends in the occurrence frequencies of the heavy precipitation during 1980–2014 (Fig. S7 online). But heavy precipitation frequency shows a significantly decreased trend (−0.5 number a^{-1}) after 1998, which is mainly caused by the decreased frequency of Type 1 (−0.4 number a^{-1}), which seems to explain the reason for the aridification tendency in the SETP since 1998 [47] in a synoptic-scale perspective. In future, the circulation changes responsible for the Type 1 frequency decreasing will be further investigated. This will be helpful for enhancing our heavy precipitation projection, disaster prevention and mitigation capabilities in the Asian water tower area.

Conflict of interest

The authors declare that they have no conflict of interest.

Acknowledgments

This study was supported by the Second Tibetan Plateau Scientific Expedition, Research (STEP) Programme (2019QZKK0105) and the National Natural Science Foundation of China (U2442213, 42122033, 42475002 and 42075006).

Author contributions

Xuelong Chen designed the study, conducted the analysis strategy and revised the draft. Dianbin Cao designed the study, conducted the analysis strategy, figure production and draft preparation. The other authors contributed to the scientific interpretation and polishing the manuscript. We appreciate the comments and suggestions from the four reviewers and Dr. Guixing Chen.

Data availability

The daily geopotential height, u and v wind, temperature and specific humidity are accessed from MERRA2 (available at https://disc.gsfc.nasa.gov/datasets/). All figures are made by NCAR Command Language (Version 6.4.0), which is available at https://www.ncl.ucar.edu/.

Fig. 3. Evolution of the composite anomalies of large-scale circulation for Type 1 and Type 2. (a1)–(a3) and (d1)–(d3) show temperature (shading, units: K), geopotential height (blue solid contours, units: gpm) and wind (vectors, units: m s^{-1}) at 500 hPa. (b1)–(b3) and (e1) –(e3) show divergence of moisture flux (shading, units: g kg^{-1} s^{-1} 10^{-4}) at 500 hPa. (c1)–(c3) and (f1)–(f3) are cross-section of the UV-wind (vectors, units: m s^{-1}) and specific humidity (shading, units: g kg^{-1}) with the climatological specific humidity (green solid contours) along the dash purple line in (b1) and (e1). Top to bottom in Type 1 and Type 2 indicate the circulation of 4 day, 2 day and 0 day before the day of heavy precipitation occurrence.

Appendix A. Supplementary material

Supplementary data to this article can be found online at https://doi.org/10.1016/j.scib.2024.12.031.

References

[1] Xu X, Lu C, Shi X, et al. World water tower: an atmospheric perspective. Geophys Res Lett 2008;35:L20815.
[2] Immerzeel WW, van Beek LPH, Bierkens MFP. Climate change will affect the Asian Water Towers. Science 2010;328:1382–5.
[3] Xu X, Zhao T, Lu C, et al. An important mechanism sustaining the atmospheric "water tower" over the Tibetan Plateau. Atmos Chem Phys 2014;14:11287–95.
[4] Kirschbaum D, Kapnick SB, Stanley T, et al. Changes in extreme precipitation and landslides over High Mountain Asia. Geophys Res Lett 2020;47:2019GL085347.
[5] Lu H, Li F, Gong T, et al. Temporal variability of precipitation over the Qinghai-Tibetan Plateau and its surrounding areas in the last 40 years. Int J Climatol 2022;43:1–23.
[6] Yao T, Bolch T, Chen D, et al. The imbalance of the Asian water tower. Nat Rev Earth Environ 2022;3:618–32.
[7] Xiong J, Yong Z, Wang Z, et al. Spatial and temporal patterns of the extreme precipitation across the Tibetan Plateau (1986–2015). Water 2019;11:1453.
[8] Zhao R, Chen B, Xu X. Intensified moisture sources of heavy precipitation events contributed to interannual trend in precipitation over the Three-Rivers-Headwater region in China. Front Earth Sci 2021;9:674037.
[9] Sun J, Yao X, Deng G, et al. Characteristics and synoptic patterns of regional extreme rainfall over the central and eastern Tibetan Plateau in boreal summer. Atmos 2021;12:379.
[10] Long Q, Chen Q, Gui K, et al. A case study of a heavy rain over the Southeastern Tibetan Plateau. Atmos 2016;7:118.
[11] Feng L, Zhou T. Water vapor transport for summer precipitation over the Tibetan Plateau. J Geophys Res Atmos 2012;117:D20114.
[12] Wang X, Pang G, Yang M. Precipitation over the Tibetan Plateau during recent decades: a review based on observations and simulations. Int J Climatol 2018;38:1116–31.
[13] Ge G, Shi Z, Yang X, et al. Analysis of precipitation extremes in the Qinghai-Tibetan Plateau, China: spatio-temporal characteristics and topography effects. Atmos 2017;8:127.
[14] Zhang H, Gao Y, Xu J, et al. Decomposition of future moisture flux changes over the Tibetan Plateau projected by global and regional climate models. J Clim 2019;32:7037–53.
[15] Tveito OE. An assessment of circulation type classifications for precipitation distribution in Norway. Phys Chem Earth Parts ABC 2010;35:395–402.
[16] Li Q, Lin Z, Zhou S, et al. Weather regimes associated with summer precipitation over the southeast Tibetan Plateau and the relationship with ENSO. Int J Climatol 2024;44:1391–408.
[17] Milrad SM, Atallah EH, Gyakum JR. Synoptic typing of extreme cool-season precipitation events at St. John's, Newfoundland, 1979–2005. Weather Forecast 2010;25:562–86.
[18] Milrad SM, Atallah EH, Gyakum JR, et al. Synoptic typing and precursors of heavy warm-season precipitation events at Montreal, Québec Weather Forecast 2014;29:419–44.
[19] Moore BJ, Mahoney KM, Sukovich EM, et al. Climatology and environmental characteristics of extreme precipitation events in the Southeastern United States. Mon Weather Rev 2015;143:718–41.
[20] You Q, Kang S, Aguilar E, et al. Changes in daily climate extremes in the eastern and central Tibetan Plateau during 1961–2005. J Geophys Res 2008;113:D07101.
[21] Loriaux JM, Lenderink G, Siebesma AP. Large-scale controls on extreme precipitation. J Clim 2017;30:955–68.
[22] Ge J, You Q, Zhang Y. The influence of the Asian summer monsoon onset on the northward movement of the South Asian high towards the Tibetan Plateau and its thermodynamic mechanism. Int J Climatol 2018;38:543–53.
[23] Yang S, Zhang W, Chen B, et al. Remote moisture sources for 6-hour summer precipitation over the Southeastern Tibetan Plateau and its effects on precipitation intensity. Atmos Res 2020;236:104803.
[24] Lai H, Chen D, Chen HW. Precipitation variability related to atmospheric circulation patterns over the Tibetan Plateau. Int J Climatol 2024;44:91–107.
[25] Liu W, Wang L, Chen D, et al. Large-scale circulation classification and its links to observed precipitation in the eastern and central Tibetan Plateau. Clim Dyn 2016;46:3481–97.
[26] Schiemann R, Lüthi D, Schär C. Seasonality and interannual variability of the westerly jet in the Tibetan Plateau region. J Clim 2009;22:2940–57.
[27] Lin Z, Yao X, Guo W, et al. Extreme precipitation events over the Tibetan Plateau and its vicinity associated with Tibetan Plateau vortices. Atmos Res 2022;280:106433.
[28] Huang W, Qiu T, Yang Z, et al. On the formation mechanism for wintertime extreme precipitation events over the Southeastern Tibetan Plateau. J Geophys Res Atmos 2018;123:12,692-12,714.
[29] He K, Liu G, Wu R, et al. Oceanic and land relay effects linking spring tropical Indian Ocean sea surface temperature and summer Tibetan Plateau precipitation. Atmos Res 2022;266:105953.
[30] Ye W, Li Y, Zhang D. Generation of extreme precipitation over the Southeastern Tibetan Plateau associated with TC Rashmi (2008). Weather Forecast 2022;37:2223–38.
[31] Zhang X, Chen D, Yao T. Evaluation of circulation-type classifications with respect to temperature and precipitation variations in the central and eastern Tibetan Plateau. Int J Climatol 2018;38:4938–49.
[32] Ning B, Yang X, Chang L. Changes of temperature and precipitation extremes in Hengduan Mountains, Qinghai-Xizang Plateau in 1961–2008. Chin Geogr Sci 2012;22:422–36.
[33] Zhang J, Zhao T, Zhou L, et al. Historical changes and future projections of extreme temperature and precipitation along the Sichuan-Xizang railway. J Meteorol Res 2021;35:402–15.
[34] Zeng C, Zhang F, Wang L, et al. Summer precipitation characteristics on the southern Tibetan Plateau. Int J Climatol 2021;41:E3160–77.
[35] Bookhagen B, Burbank DW. Topography, relief, and TRMM-derived rainfall variations along the Himalaya. Geophys Res Lett 2006;33:L08405.
[36] Zhang X-L, Wang S-J, Zhang J-M, et al. Temporal and spatial variability in precipitation trends in the Southeast Tibetan Plateau during 1961–2012. Clim Past Discuss 2015;11:447–87.
[37] Zhang X, Yao X, Ma J, et al. Climatology of transverse shear lines related to heavy rainfall over the Tibetan Plateau during boreal summer. J Meteorol Res 2016;30:915–26.
[38] Qiu T, Huang W, Wright JS, et al. Moisture sources for wintertime intense precipitation events over the three snowy subregions of the Tibetan Plateau. J Geophys Res Atmos 2019;124:12708–25.
[39] Ayantobo OO, Wei J, Hou M, et al. Characterizing potential sources and transport pathways of intense moisture during extreme precipitation events over the Tibetan Plateau. J Hydrol 2022;615:128734.
[40] Chen X, Cao D, Liu Y, et al. An observational view of rainfall characteristics and evaluation of ERA5 diurnal cycle in the Yarlung Tsangbo Grand Canyon. China Q J R Meteorol Soc 2023;149:1459–72.
[41] Zhu Y, Yang S. Evaluation of CMIP6 for historical temperature and precipitation over the Tibetan Plateau and its comparison with CMIP5. Adv Clim Change Res 2020;11:239–51.
[42] Gao J, Du J, Yang C, et al. Evaluation and correction of climate simulations for the Tibetan Plateau using the CMIP6 models. Atmos 2022;13:1947.
[43] Zeng J, Huang A, Wu P, et al. Typical synoptic patterns responsible for summer regional hourly extreme precipitation events over the middle and lower Yangtze River Basin. China Geophys Res Lett 2023;50:e2023GL104829.
[44] Lin Z, Guo W, Jia L, et al. Climatology of Tibetan Plateau vortices derived from multiple reanalysis datasets. Clim Dyn 2020;55:2237–52.
[45] Wu G, Tang Y, He B, et al. Potential vorticity perspective of the genesis of a Tibetan Plateau vortex in June 2016. Clim Dyn 2022;58:3351–67.
[46] Gelaro R, McCarty W, Suárez M, et al. The Modern-Era retrospective analysis for research and applications, version 2 (MERRA-2). J Clim 2017;30:5419–54.
[47] Li L, Zhang R, Wen M, et al. Regionally different precipitation trends over the Tibetan Plateau in the warming context: a perspective of the Tibetan Plateau vortices. Geophys Res Lett 2021;48:2020GL091680.
[48] Zhang G, Mao J, Wu G, et al. Impact of potential vorticity anomalies around the eastern Tibetan Plateau on quasi-biweekly oscillations of summer rainfall within and south of the Yangtze Basin in 2016. Clim Dyn 2021;56:813–35.
[49] Zhao Y, Xu X, Li J, et al. The large-scale circulation patterns responsible for extreme precipitation over the North China plain in midsummer. J Geophys Res Atmos 2019;124:12794–809.
[50] Hu Y, Deng Y, Zhou Z, et al. A statistical and dynamical characterization of large-scale circulation patterns associated with summer extreme precipitation over the middle reaches of Yangtze river. Clim Dyn 2019;52:6213–28.
[51] Park T-W, Ho C-H, Deng Y. A synoptic and dynamical characterization of wave-train and blocking cold surge over East Asia. Clim Dyn 2014;43:753–70.
[52] Zhao S, Deng Y, Black RX. A dynamical and statistical characterization of U.S. extreme precipitation events and their associated large-scale meteorological patterns. J Clim 2017;30:1307–26.
[53] Zhao D, Dong W, Lin Y, et al. Diurnal variation of precipitation over the high mountain Asia: spatial distribution and its seasonality. J Hydrometeorol 2022;23:1945–59.
[54] Ward JH. Hierarchical grouping to optimize an objective function. J Am Stat Assoc 1963;58:236–44.
[55] Zhao Y, Li J, Ren L, et al. Fine-scale characteristics and dominant synoptic factors of spring precipitation over complex terrain of the southeastern Tibetan Plateau. J Geophys Res Atmos 2023;128:e2022JD038352.
[56] Holton JR. An introduction to dynamic meteorology. 4th ed. Burlington: Elsevier Academic Press; 2004.
[57] Lin Z, Guo W, Yao X, et al. Tibetan Plateau vortex-associated precipitation and its link with the Tibetan Plateau heating anomaly. Int J Climatol 2021;41:6300–13.
[58] Wu G, Zheng Y, Liu Y. Dynamical and thermal problems in vortex development and movement. Part II: generalized slantwise vorticity development. Acta Meteorol Sin 2013;27:15–25.
[59] Dong W, Lin Y, Wright JS, et al. Summer rainfall over the southwestern Tibetan Plateau controlled by deep convection over the Indian subcontinent. Nat Commun 2016;7:10925.
[60] Chen L, Chen B, Zhao R, et al. Characterizing the synoptic-scale precursors of extreme precipitation events in the southeastern edge of the Tibetan Plateau: anomalous evolution of atmospheric dynamic-thermal structure. Water 2023;15:1407.